Lidar Network Observations of Cirrus Morphological and Scattering Properties during the International Cirrus Experiment 1989: The 18 October 1989 Case Study and Statistical Analysis

ALBERT ANSMANN,* JENS BÖSENBERG,† GÉRARD BROGNIEZ,# SALEM ELOURAGINI,@ PIERRE H. FLAMANT,@ KARLHEINZ KLAPHECK,& HOLGER LINN,† LOUIS MENENGER,@ WALFRIED MICHAELIS,* MAREN RIEBESELL,* CHRISTOPH SENFF,† PIERRE-YVES THRO,† ULLA WANDINGER,* AND CLAUS WEITKAMP*

*Institut für Physik, GKSS-Forschungszentrum Geesthacht GmbH, Geesthacht, Germany
†Max-Planck-Institut für Meteorologie, Hamburg, Germany
#Laboratoire d'Optique Atmosphérique, Université des Sciences et Techniques de Lille Flandres Artois, Lille, France
@Laboratoire de Météorologie Dynamique, Ecole Polytechnique, Palaiseau, France
&Meteorologisches Observatorium Hamburg, Deutscher Wetterdienst, Hamburg, Germany

(Manuscript received 14 September 1992, in final form 26 February 1993)

ABSTRACT

Four lidars, located roughly 75 km from each other in the inner German Bight of the North Sea, were used to measure geometrical and optical properties of cirrus clouds during the International Cirrus Experiment 1989 (ICE '89). A complete cirrus life cycle was observed simultaneously with three lidars during a case study on 18 October 1989. Time series of particle backscatter, depolarization-ratio height profiles, cloud depth, optical thickness, and of the cirrus extinction-to-backscatter, or lidar, ratio describe the evolution of the cloud system. A two-wavelength lidar measurement was performed and indicates wavelength independence of ice-crystal scattering. The optical and geometrical depths of the cirrus were well correlated and varied between 0.01 and 0.5 and 100 m and 4.5 km, respectively. Although the evolution of the cloud deck was similar over the different observation sites, cirrus geometrical, scattering, and microphysical properties were found to vary considerably within the lidar network. A statistical analysis of ice-cloud properties is performed based on 38 different cirrus cases sampled during ICE '89. Cirrus formation was found to start at the tropopause in most cases. Ice clouds, measured at high midlatitudes (around 54°N), were thin with mean optical and geometrical depths mainly below 0.4 and 2 km, respectively. A good correlation between mean cloud optical and geometrical thickness, and a weak decrease of the mean optical depths with temperature was observed.

1. Introduction

Numerical simulation studies show that high-altitude ice clouds have a large influence on weather and climate and that intensive measurements of the relationship between the radiative and microphysical properties of cirrus clouds and the meteorological state of the ambient air are needed (Liou 1986). For an improved understanding of the formation, subsistence, and dissipation, that is, of the life cycle of cirrus clouds, extended studies are necessary. Two such studies have already been performed in regional experiments, the First International Satellite Cloud Climatology Project (ISCCP) Regional Experiment (FIRE, see *Monthly Weather Review*, Vol. **118**, No. 11, 1990) and the International Cirrus Experiment (ICE, Raschke et al. 1990), during which measurements have been made from a diverse set of observing platforms including research aircraft and ground-based measurement networks.

In order to determine morphological and scattering characteristics of ice clouds such as cloud top and base heights, the evolution of the height-dependent cloud structure, and cirrus vertical and optical depths with high temporal and spatial resolution, mesoscale lidar nets were installed during both campaigns (Sassen et al. 1990; Bösenberg et al. 1990). The ICE network consisted of four lidars located in and around the German Bight (53.5°–55°N, 7°–9°E) of the North Sea area at roughly 75 km in distance from each other. For the first time an intensive field observation took place at relatively high latitudes. Cirrus clouds had already been investigated in tropical regions or at midlatitudes around 40°N and 40°S in several comprehensive studies (see Liou 1986 for an overview; Platt et al. 1987; Platt et al. 1989) and during FIRE in 1986.

In contrast to FIRE, ICE '89 was carried out with a combined Raman elastic-backscatter lidar and a differential absorption lidar (DIAL) included in the network. The combined lidar of GKSS-Forschungs-

Corresponding author address: Dr. Claus Weitkamp, Institut für Physik, GKSS, Postfach 1160, Geesthacht, FRG, D-21494.

zentrum Geesthacht (GKSS) allows the separate depth-resolved determination of cirrus extinction and backscatter coefficients at nighttime, and thus of the cirrus extinction-to-backscatter, or lidar, ratio. As far as we know, this is the first time that cirrus lidar-ratio height profiles have been determined. In addition, the observations with the combined lidar allow us to analyze the reliability of cirrus extinction and backscattering profiling with elastic backscatter lidars (Ansmann et al. 1992b). Finally, and also for the first time, to the authors' best knowledge, several lidar measurements of cirrus humidity at temperatures below −40°C were taken with the GKSS Raman lidar (Bösenberg et al. 1990; Ansmann et al. 1992a).

With the DIAL of the Max-Planck-Institut für Meteorologie (MPI), backscatter signals are obtained simultaneously at different wavelengths in the visible. The MPI lidar thus permits the determination of the wavelength dependence of ice-crystal scattering in the short-wavelength region. Such a measurement is useful because the lidar network covers a wavelength range between 308 and 1064 nm.

The network was completed by the polarization lidar of the Meteorologisches Observatorium Hamburg, Deutscher Wetterdienst (DWD), and the mobile backscatter lidar of the Laboratoire de Météorologie Dynamique, Ecole Polytechnique, Palaiseau (LMD). The polarization lidar provides additional information on the internal structure and dynamic behavior of a cloud system.

Results of a cirrus case study are presented in this paper. On 18 October 1989 a unique dataset was collected in which a complete life cycle of a cirrus cloud system could be monitored. A cloud deck covered the entire experimental area for more than 5 h. The evolution of the cloud structures is described in terms of time series of lidar backscatter and depolarization-ratio data, cloud optical and geometrical depths, and mean aerosol extinction-to-backscatter ratios. Before the presentation of results in section 5, field sites, lidar systems, and evaluation techniques are briefly described in sections 2 to 4.

The ICE lidar observations lasted nearly two months, considerably longer than FIRE IFO (intensive field observation), and, we believe, long enough for results of a statistical analysis of the entire cirrus dataset to be representative for the location and the season. These results are discussed in section 6. During the September and October 1989 ICE campaign, 38 different cirrus cases were observed with one or several instruments of the lidar network.

2. Field sites

ICE IFO took place between 17 September and 20 October 1989. Lidar measurements were made between 5 September and 27 October 1989. The southern part of the North Sea was chosen as the experimental area; Fig. 1 shows a map of the region. The ICE operation center was located at Nordholz airfield, which was also used as the base of the research aircraft. A surface network established in and around the German Bight consisted of the stations at Nordholz and on the islands of Sylt, Heligoland, and Norderney and the research vessel *Poseidon* cruising between 54° and 56°N and 3° and 7°E. The four ground-based lidars were located at Nordholz and the North Sea islands. So, for most of the stations and for the prevailing westerly winds, the cloud systems approached from fairly homogeneous terrain, namely, from the North Sea, and were thus not disturbed by orographic effects. To provide information on the state of the atmosphere within the mesoscale net, radiosondes were launched at the Sylt, Heligoland, and Norderney sites, and from the research vessel. Vaisala RS 80 sondes were used to measure temperature, pressure, and humidity; the stations at Sylt and on board the ship provided wind information as well. Radiometric measurements were performed at Sylt, Heligoland, Nordholz, and on board the ship. A cloud camera (camera with a fish-eye lens) used to document the cloudiness of the sky was installed on the roof of the lidar trailer on Heligoland.

3. Instrumentation

The key features of the four lidars are listed in Table 1. The systems are technically quite different and in particular use different wavelengths, as they had been designed for different purposes long before ICE. A brief description of each system is given below. During the field campaign all four lidars routinely pointed exactly into the zenith to make the results comparable. At a

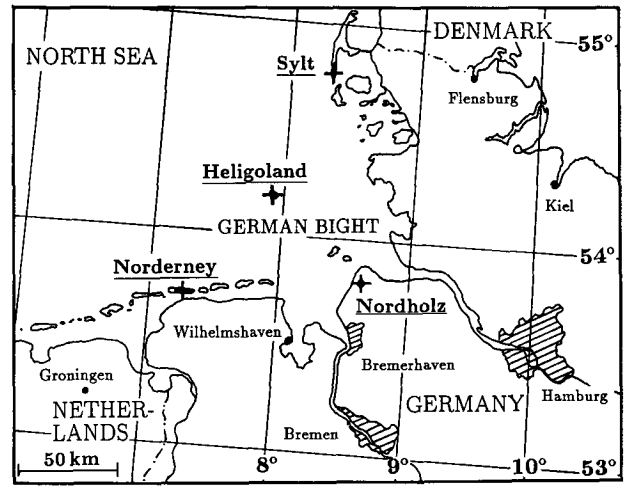

FIG. 1. Experiment area of ICE '89. Four ground-based lidars (+) were located at the ICE operation center Nordholz airfield (53.77°N, 8.67°E; LMD) and on the North Sea islands of Sylt (54.75°N, 8.30°E; MPI), Heligoland (54.19°N, 7.91°E; DWD), and Norderney (53.72°N, 7.22°E; GKSS). Radiosondes were launched at Sylt, Heligoland, and Norderney.

zenith angle of around 0° (±3 mrad), in turn, the most interesting results may be obtained with a polarization lidar as well as a combined Raman elastic-backscatter lidar because layers with falling ice crystals can be identified as such (Thomas et al. 1990). On the other hand, specular reflection by exactly horizontally oriented particles may somewhat affect the determination of height profiles of cirrus scattering coefficients, and, as a consequence, of cirrus morphology.

a. MPI DIAL

The lidar system of the Max-Planck-Institut für Meteorologie (Bösenberg 1991; Theopold and Bösenberg 1993) was initially developed for the measurement of water vapor in the lower troposphere by use of the DIAL technique. However, it is suited for backscatter measurements at cirrus levels as well. Retrieval of water vapor profiles in the upper troposphere is at the limits of the present system.

The system basically consists of two excimer-pumped dye lasers with intracavity etalon for narrow-bandwidth operation. The tunability has been used in the present experiment to investigate the wavelength dependence of cirrus scattering properties. The lasers are fired with a delay of 200 μs, so the atmosphere can be considered frozen, and backscatter and extinction do not vary between pulses. After detection with a photomultiplier and digitization with a 12-bit 20-MHz transient recorder (corresponding to 7.5-m height resolution), 100 pairs of backscatter signals are typically averaged and stored on magnetic tape. Additional averaging in height and time is applied to improve the signal-to-noise ratio.

b. DWD polarization lidar

The polarization lidar of the Meteorologisches Observatorium Hamburg of Deutscher Wetterdienst uses a ruby laser emitting at 694 nm. Transmitter and receiver are swivel mounted with an angle resolution of 0.1°; elevation range is 0°–90°, azimuth range is 220°. The scanning capability allows the recording of cloud cross sections.

The parallel and cross-polarized components of the backscattered light are separated with a polarizing beamsplitter and registered with two photomultipliers and a two-channel transient recorder. The maximum sampling rate of 100 MHz corresponds to a resolution of 1.5 m. In order to smooth the signals and to compress the data storage, a reduction to 15 m immediately after acquisition is implemented. Digital resolution of the input voltage range is 8 bits. Because of the high pulse energy of the ruby laser, a single shot gives a good-quality signal profile so that changes of cloud formation can be observed with a time resolution of a few seconds.

c. GKSS combined Raman elastic-backscatter lidar

The combined Raman elastic-backscatter lidar of GKSS (Ansmann et al. 1992a) uses a powerful XeCl excimer laser. The backscattered radiation at 308 nm (elastic Rayleigh and particle backscatter), 332 nm

TABLE 1. Instrumentation.

Institute	MPI	DWD	LMD	GKSS
ICE IFO site	Sylt	Heligoland	Nordholz	Norderney
Lidar system	DIAL	Polarization lidar	Backscatter lidar	Combined lidar
Transmitter				
Laser type	Dye	Ruby	Nd:YAG	Excimer
Wavelength (nm)	725 550	694	1064	308 (primary) 332 (N_2—Raman) 347 (H_2O—Raman)
Pulse energy (J)	0.035	2	0.050	0.270
Repetition rate (Hz)	12	1	10	250
Beam divergence (mrad)	0.1	1.2	1.0	≤0.1
Receiver				
Main mirror diameter (m)	0.5	0.3	0.3	0.8
Field of view (mrad)	0.5	1–3	2	0.2
Scanning capability	no	yes	yes	no
Cirrus properties measured				
Height, depth, structure	yes	yes	yes	yes
Backscatter profile β	yes	yes	yes	yes
Extinction profile α	no	no	no	yes (at night)
Lidar ratio profile	no	no	no	yes (at night)
Optical depth	yes	yes	yes	yes
Wavelength dependence of β	yes	no	no	no
Depolarization ratio profile	no	yes	no	no
Water vapor profile	no	no	no	yes (at night)

(nitrogen Raman backscatter), and 347 nm (water vapor Raman backscatter) is detected by photomultipliers operated in the photon counting mode. For the separation of the three wavelengths, a polychromator with interference filters is used. A multichannel scaler registers the pulses at a maximum sampling rate of 10 MHz corresponding to a depth resolution of 15 m. During ICE '89 the backscatter signals were accumulated in 60-m height intervals up to an altitude of 18 km and in time intervals of one minute or more. The count rates are corrected for photomultiplier dead time and, in the case of daytime measurements or water vapor observations at nighttime, for background noise. For the determination of the mean sky background, the data from the height range between 16 and 18 km are taken.

d. LMD elastic-backscatter lidar

During ICE '89, the LMD group used an elastic-backscatter lidar. A Nd:YAG laser transmits light at 1.064 μm. Return signals are digitized with a 12-bit transient recorder. The maximum spatial resolution of the one-channel system is 30 m. Because the lidar system had been designed for boundary-layer and low-cloud studies, the measurements taken on cirrus during ICE '89 are still noisy even after averaging several hundred shots. So, only cloud-base and cloud-top heights could be determined most of the time. The narrow field-of-view infrared radiometer (Barnes PRT 5) of the Laboratoire d'Optique Atmosphérique was installed next to the LMD lidar.

4. Background of elastic-backscatter signal evaluation

The parameters determined with the lidars during ICE '89 are listed in Table 1. In this section only methods for the treatment of elastic backscatter signals are discussed because cirrus scattering properties presented in the following sections are exclusively derived from elastic backscatter data. The applied techniques are developed by starting from the basic lidar equation

$$P(z) = Cz^{-2}[\beta_{aer}(z) + \beta_{mol}(z)] \times \exp\left\{-2\int_0^z [\alpha_{aer}(\zeta) + \alpha_{mol}(\zeta)]d\zeta\right\}; \quad (1)$$

$P(z)$ is the power received from distance z; C contains all depth-independent system parameters; $\beta_{aer}(z)$ and $\beta_{mol}(z)$ are the backscatter coefficients for aerosol and molecular (Rayleigh) scattering, respectively. The coefficients $\alpha_{aer}(z)$ and $\alpha_{mol}(z)$ describe the extinction due to particle scattering and molecular absorption and scattering.

a. Cirrus geometrical properties

In the present study, an aerosol layer at high altitudes and correspondingly low temperatures, commonly below −25°C, is called a cirrus cloud if

$$\beta_{aer}(z) \geq 4\beta_{mol}(z) \quad (2)$$

for the wavelength of $\lambda = 530$ nm. For the different measurement wavelengths between 308 and 1064 nm the corresponding condition is found by assuming a proportionality to λ^{-4} for Rayleigh and λ^0 for ice-crystal scattering. The neglection of the spectral dependence of particle scattering in cirrus holds if the size of the crystals is large compared to the measurement wavelength (van de Hulst 1981). This is usually the case for cirrus and has been confirmed by the observation with the DIAL. The determination of $\beta_{aer}(z)$ and $\beta_{mol}(z)$ is explained below. In general, no major problem occurred with the arbitrarily chosen definition (2), perhaps with the exception of the analysis of data sampled with the LMD lidar at Nordholz because Rayleigh scattering intensity at a wavelength of 1.06 μm is below the detection limit of the system. Consequently, this group defined as a cirrus any region at high altitude with a signal level significantly above the detection limit.

b. Cirrus extinction and backscatter properties

Cirrus optical properties are obtained by solving a Bernoulli equation derived from the basic lidar equation (1). The solution for the backscatter coefficient is (Fernald 1984)

$$\beta_{aer}(z) = -\beta_{mol}(z) + \frac{A(z_0, z)}{B(z_0) - 2S_{aer}\int_{z_0}^{z} A(z_0, \zeta)d\zeta}, \quad (3)$$

with

$$A(z_0, x) = P(x)x^2 \times \exp\left[-2(S_{aer} - S_{mol})\int_{z_0}^{x} \beta_{mol}(\xi)d\xi\right], \quad (4)$$

and

$$B(z_0) = \frac{P(z_0)z_0^2}{\beta_{aer}(z_0) + \beta_{mol}(z_0)}; \quad (5)$$

$S_{mol} = 8\pi/3$ sr is the molecular extinction-to-backscatter ratio. The aerosol lidar ratio S_{aer} and the particle backscatter coefficient $\beta_{aer}(z_0)$ at a specific range z_0 must be estimated. In addition, the height profile of Rayleigh backscattering $\beta_{mol}(z)$ must be known and is usually determined with sufficient accuracy from a standard atmosphere model or, if available, from actual radiosonde data of pressure and temperature.

Equation (3) assumes only particle and Rayleigh scattering. Ozone absorption, which is not negligible at $\lambda = 308$ nm of the combined lidar, must be corrected before applying the formalism. This is done by using a standard ozone density model. The relative error of the scattering parameters introduced by the ozone density estimate is of the order of 10%–20% for cirrus optical depths between 0.2 and 0.5 (Ansmann et al. 1992b). For laser wavelengths 694 nm and larger, molecular scattering within the cirrus can be ignored. Then $A(z_0, z)$ reduces to the range-corrected lidar signal $P(z)z^2$, and the molecular scattering terms vanish. At $\lambda = 308$ nm, Rayleigh scattering always represents a major contribution.

Equation (3) can in principle be integrated by starting from the reference height z_0, which may be either the near end ($z > z_0$, forward integration) or the remote end of the measuring range ($z < z_0$, backward integration). Numerical stability, however, is only given in the backward integration case (Klett 1981). An appropriate range-averaged cloud lidar ratio may be determined if both forward and backward integration modes can be applied, provided that $\beta_{aer}(z_0)$ below and above the cloud is well estimated (Ansmann et al. 1992b). In the case of cirrus scattering profiling, the influence of the boundary-value estimate $\beta_{aer}(z_0)$ on the result is fortunately small because air is typically clear in the free troposphere most of the time (Russel et al. 1979) so that $\beta_{aer}(z_0) = 0$ can be assumed outside cirrus without leading to large errors. Such an assumption does not apply if a wavelength of $\lambda = 1.06$ μm is used because the weak Rayleigh scattering does not allow the use of regions of pure Rayleigh scattering for calibration. The reference height z_0 must be located inside the cloud or in another aerosol layer, for example, in the boundary layer.

The sensitivity of forward integration to S_{aer} alone can be used to determine the cloud lidar ratio (Platt 1979). This is useful if the signal-to-noise ratio at heights above the ice cloud is too small for a proper backward integration. The numerical calculations of Platt (1979) and the measurements with the combined lidar at Norderney show that for cirrus having an optical depth between 0.2 and 0.5, the mean cloud lidar ratio is roughly one-half of the extinction-to-backscatter ratio for which forward integration gets unstable. The technique is applied in section 5 in the evaluation of lidar data measured at Heligoland. It cannot be used if the cirrus is optically very thin because then forward integration is always stable.

Together with the cloud lidar ratio, the cirrus optical depth

$$\delta = S_{aer} \int_{z_b}^{z_t} \beta_{aer}(z)dz \tag{6}$$

with cloud-base and cloud-top heights z_b and z_t is determined. The height profile of the cirrus extinction coefficient $S_{aer}\beta_{aer}(z)$ is, however, not reliable due to the range dependence of the true lidar ratio (Ansmann et al. 1992b).

c. Depolarization ratio

The depolarization ratio is defined as [Schotland et al. (1971), cf. lidar equation (1)]

$$\Delta(z) = \frac{C_{\parallel}}{C_{\perp}} \frac{P_{\perp}(z)}{P_{\parallel}(z)}. \tag{7}$$

The subscripts $\perp$ and $\parallel$ stand for measurements made with the plane of polarization of the receiver perpendicular and parallel to that of the laser, respectively. The ratio $C_{\parallel}/C_{\perp}$ is deduced from measured properties of the spectrometer. If $\beta_{aer}(z) \gg \beta_{mol}(z)$ in clouds and equal atmospheric transmission for both lidar return components is assumed, $\Delta(z)$ is equal to the backscatter ratio $\beta_{\perp,aer}(z)/\beta_{\parallel,aer}(z)$. In cirrus, a backscatter component $\beta_{\perp,aer} > 0$ is caused by multiple internal reflections in ice crystals.

d. Wavelength dependence of ice-crystal scattering

To prove the λ^0 dependence of cirrus particle scattering, a simultaneous measurement of lidar returns at the wavelengths $\lambda_1 = 550$ nm and $\lambda_2 = 728$ nm was made. By assuming $\beta_{aer}(z) \gg \beta_{mol}(z)$ inside the cloud for $\lambda \geqslant 550$ nm and by neglecting the small difference of a few percent between the Rayleigh transmissions at 550 and 728 nm, the signal ratio can be expressed according to (1) by

$$\frac{P(z, \lambda_1)}{P(z, \lambda_2)} = \frac{C(\lambda_1)\beta_{aer}(z, \lambda_1) \exp\left\{-2 \int_0^z \alpha_{aer}(\zeta, \lambda_1)d\zeta\right\}}{C(\lambda_2)\beta_{aer}(z, \lambda_2) \exp\left\{-2 \int_0^z \alpha_{aer}(\zeta, \lambda_2)d\zeta\right\}}. \tag{8}$$

In the case of a weakly attenuating cirrus with an optical depth $\delta \leqslant 0.2$ and a small wavelength dependence of particle scattering, the signal ratio depends only on the backscatter coefficient ratio because the transmission ratio is approximately range independent inside the cirrus. If ice-crystal scattering is wavelength independent, as it is expected to be, the signal ratio is constant with height, independent of the cirrus optical depth. A further discussion of the topic is given in section 5c.

5. 18 October 1989 cirrus case study

A complete life cycle of a cirrus cloud system was observed on 18 October 1989. A closed cirrus deck covering the entire experimental area was present between about 7.5 km and the tropopause at 11.6 km

height for 5–9 h. The cloud field formed in the morning, persisted for several hours, and dissolved in the evening.

A large number of experiments were made on that day. In addition to the lidar and radiosonde observations, satellite, airborne, and ground-based radiometer data were collected to determine radiative properties of cirrus. Aircraft measurements were made to investigate microphysical properties and ambient air conditions.

a. Meteorological situation

An overview of the air motion in the upper troposphere at 1200 UTC 18 October 1989 is shown in Fig. 2. As can be seen, the jet stream was oriented in a southwest–northeast direction over the northern North Sea. A high pressure ridge, which determined the weather in the experimental area, was located over the central part of Europe. The ridge moved slowly eastward during the day. Low wind speeds between 10 and 15 m s^{-1} prevailed in the upper troposphere over the southern part of the North Sea. During the morning hours a moist and warm air mass reached the North Sea area from the south at heights above 8 km.

Radiosonde observations indicated a stable stratification in the upper troposphere over all three islands with a temperature lapse rate of about 7°C km^{-1} in the cirrus cloud layer. Temperatures ranged from −40° to −60°C between about 8.5 km and the tropopause height at 11.6 km. Although radiosonde measurements exhibited a moist layer above the 9-km height in the morning and a lowering of the layer base height during the day attributed to the evaporation of descending ice-crystal trails, the recorded humidity values cannot be used for a quantitative statement. An error analysis based on 131 radiosonde ascents performed at Sylt (93 ascents) and Norderney (38 ascents) and on accompanying lidar measurements, indicating whether cirrus was present or not, shows that the radiosondes typically measured values between 80% and 95% relative humidity related to ice at −40°C, between 70% and 85% at −50°C, and between 60% and 80% at −60°C in cirrus cloud layers instead of 100%. This finding is supported by cirrus humidity measurements with the Raman lidar (Bösenberg et al. 1990; Ansmann et al. 1992b). During the passage of a cirrostratus system, for example, the lidar observation indicated saturation over ice in the main layer of a cirrostratus deck, that is, above the ice virga region, at temperatures below −50°C, while the relative humidity measured with the radiosonde was only 60% of the lidar value.

The satellite image in Fig. 3 shows that most parts of the southern North Sea area were covered by cirrus clouds at 1230 UTC 18 October 1989. A cloud-free band extended over the middle part of the North Sea. To the north and northwest of this band, contrails indicated by straight lines occured west of Denmark and east of England. The horizontally inhomogeneous cirrostratus was optically relatively thick over Norderney and Heligoland, and thin over the Sylt site.

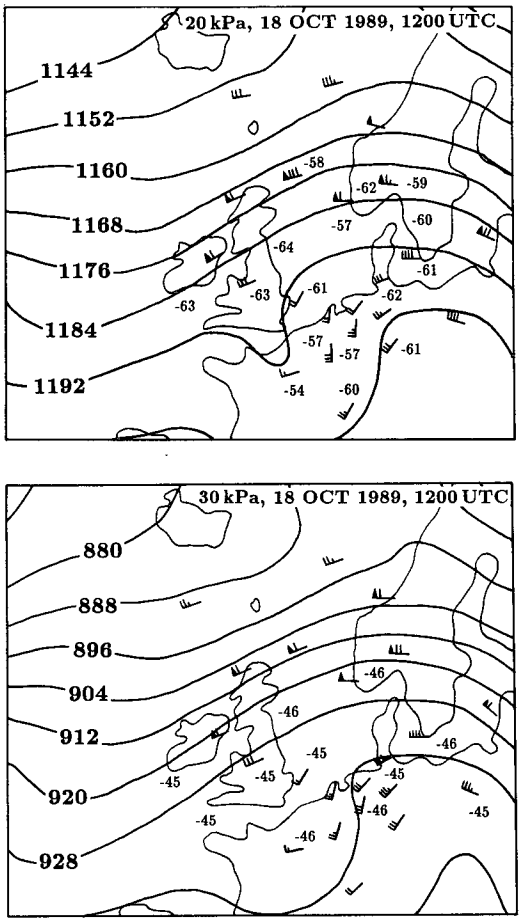

FIG. 2. Isobaric analysis (20 kPa, 30 kPa) of geopotential heights (solid lines) for 1200 UTC 18 October 1989. Also indicated are temperatures (°C), horizontal wind direction (arrows), and wind speed. Small and large barbs and triangles at the arrows stand for wind velocities of 2.5, 5, and 25 m s^{-1}, respectively.

b. Cirrus structure

Figure 4 shows time–height sections of the cirrus cover observed over the islands of Sylt, Heligoland, and Norderney. Unfortunately, the LMD lidar at Nordholz could not fully contribute to this case study. Forward (Sylt) and backward (Norderney) integration is applied in the determination of the backscatter coefficient. The use of a time-independent lidar ratio of 10 sr is appropriate for the study of cirrus morphological characteristics. The cirrus over Heligoland is shown in terms of 10 $\log[P(z)z^2]$. The range-corrected signal $P(z)z^2$ is proportional to the particle backscatter coefficient according to (1), if a small decrease of the transmission with height and weak Rayleigh backscattering are neglected. Values of 0, 5, 10, and 25 dB correspond

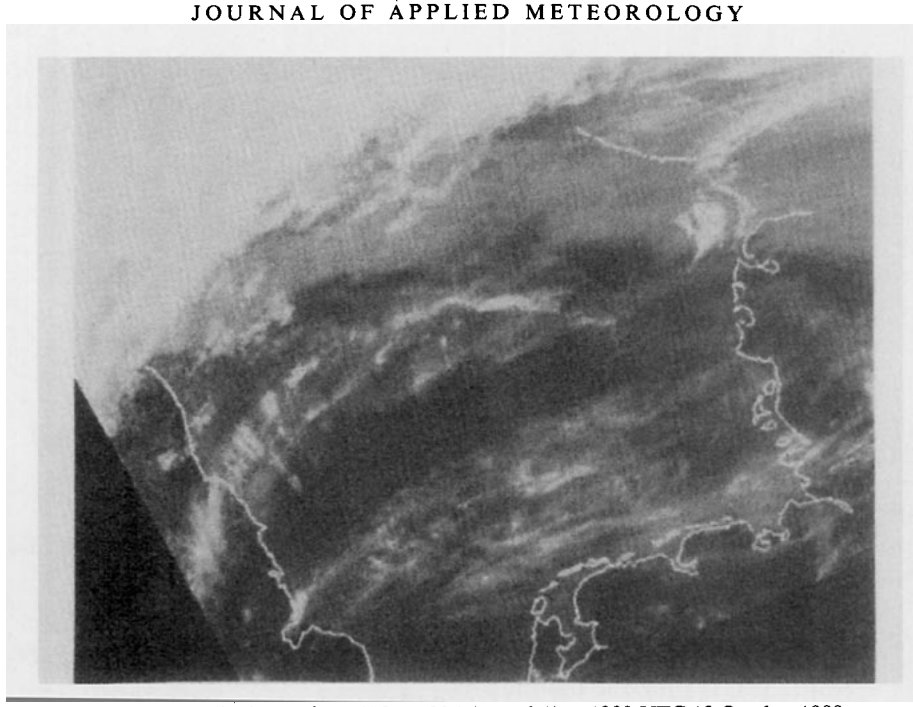

FIG. 3. Satellite image from *NOAA-11* (channel 4) at 1230 UTC 18 October 1989.

to backscatter coefficients of 2.15×10^{-4}, 6.79×10^{-4}, 2.15×10^{-3}, and 6.79×10^{-2} km^{-1} sr^{-1}, respectively. White columns in Fig. 4 indicate measurement breaks.

A closed deck was measured for more than 8, 7, and 5 hours over Sylt, Heligoland, and Norderney, respectively. Cloud formation began in the morning at about 0830 UTC (Norderney), 0945 UTC (Heligoland), and 1045 UTC (Sylt). The occurrence of first ice clouds over Heligoland and Sylt 75 and 135 min after the appearance of cirrus over Norderney is consistent with the displacement of a warm front moving east-northeast with a velocity of 11.5 m s^{-1} (cf. Figs. 1 and 2).

First, thin cirrus clouds appeared in the upper part of the moist layer just below the tropopause. The tropopause was found at 11.6 km at all three stations. A rapid increase of the vertical extent of the cloud layer was observed over Norderney and Heligoland and a steady but slow increase over Sylt. While the top of the cloud deck stayed approximately constant, the base height lowered in time to heights of, on average, 9 km at Norderney, 8–8.5 km at Heligoland, and below 7.5 km at Sylt. At Nordholz, the cloud base was found between 8.5 and 9.0 km during the measurement period from 1100 to 1400 UTC.

The cloud deck was inhomogeneous, with holes mainly in the upper part of the cirrus. The inhomogeneities and the successive lowering of the cloud base were caused by ice crystals falling out of the cloud before they completely evaporated. Fallstreaks and broadened contrails were observed by eye during the whole day.

The cirrostratus was optically thin. Maximum values of the optical depth of 0.4–0.5 were measured in the middle of the observation period between 1245 and 1315 UTC (Norderney), 1315 and 1415 UTC (Heligoland), and 1400 and 1500 UTC (Sylt).

At Nordholz, maximum values of the IR cirrus emissivity, measured with a radiometer, were observed between 1330 and 1400 UTC. Enhanced emissivity due to high-altitude clouds was measured between 1030 and 1630 UTC.

Figure 5 shows a short measurement section in terms of the cirrus IR optical depth δ_{IR} derived from the radiometer data; δ_{IR} is a factor of 2–3 smaller than the visible and near-IR optical depth (Platt 1979; Platt et al. 1987). Thus, the maximum visible cirrus optical depth, observed at Nordholz at 1340 UTC, was roughly between 0.3 and 0.45.

In Fig. 5 a height profile of the near-IR backscatter coefficient $\beta_{aer}(z)$ is shown. The backward integration method is applied and the boundary value $\beta_{aer}(z_0)$ is varied until $2\delta_{IR} = S_{aer} \int_{z_1}^{z_2} \beta_{aer}(z)dz$ with $S_{aer} = 10$ sr, $z_1 = 9$ km, and $z_2 = 10$ km. The determined maximum backscatter value of 0.045 km^{-1} sr^{-1} at 9.5 km agrees with the results shown in Fig. 4.

The dissolution of the cloud deck was characterized at all three islands by a lowering of the top height and a rapid increase of the base height. Finally, a large cloud segment reaching down to about 7.5 km passed the receiver field of view. A few isolated small cirrus clouds were observed between 7 and 11 km toward the end of the measurement.

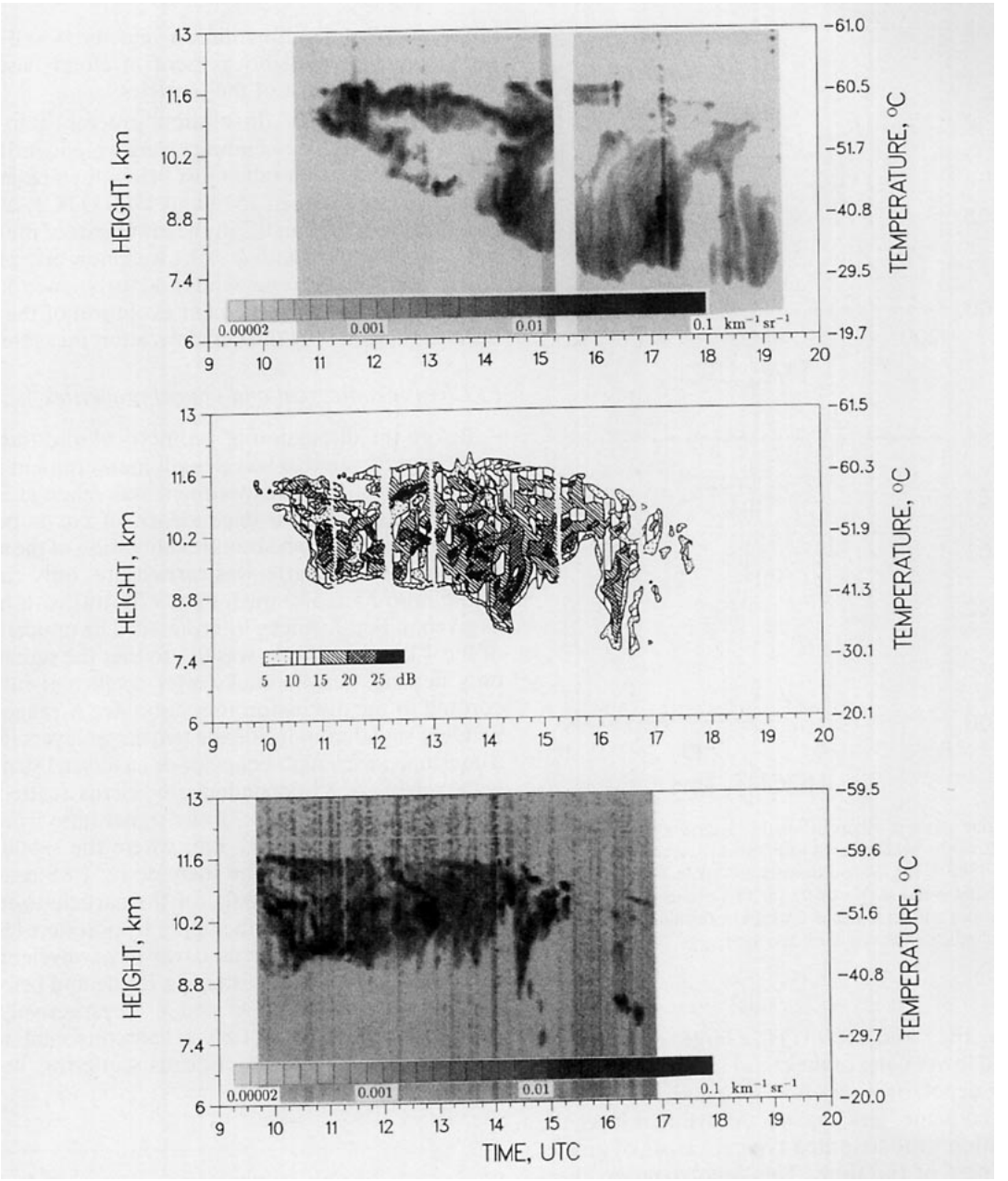

FIG. 4. Cirrus cloud deck observed at the Sylt (top), Heligoland (middle), and Norderney site (bottom) on 18 October 1989. The range-corrected signal (Heligoland) and the backscatter coefficient are shown. Time and range resolution are 180 s and 75 m (Sylt), 120 s and 15 m (Heligoland), and 180 s and 60 m (Norderney). The temperature, indicated on the right-hand scale, was measured with radiosondes at the corresponding stations between 1315 and 1415 UTC.

More details of the cloud structure and information about the microphysical properties and the internal dynamic behavior of the cirrostratus can be inferred from Fig. 6, in which an overview of the depolarization-ratio measurement is given. The corresponding height–time display of the backscatter signal is shown in Fig. 4. During cirrus formation, $\Delta < 0.1$ dominated in the upper part of the cloud, probably caused by descending layers. Such low values of Δ can best be explained by specular reflection from falling, horizontally oriented crystals (Liou and Lahore 1974). Low depolarization was also observed along the leading edge of fallstreaks which caused a rapid increase of cloud depth. Depolarization ratios were typically greater than 0.2 at the lower cloud rim most of the time owing to suspended and thus randomly oriented ice crystals.

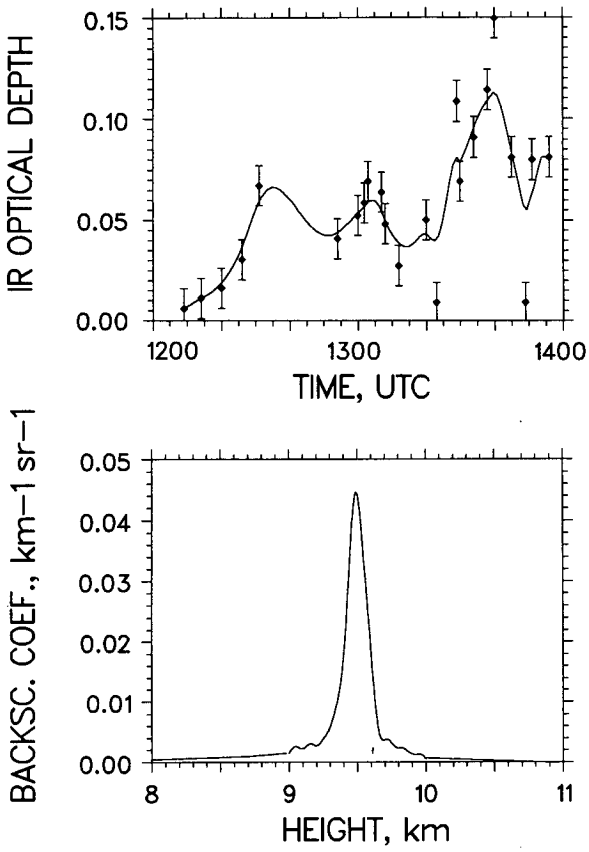

FIG. 5. Time series of cirrus infrared (11 μm) optical depth and height profile of the near-infrared (1.06 μm) backscatter coefficient observed at 1300 UTC. Measurements are taken with radiometer and lidar, respectively, at Nordholz on 18 October 1989. A cubic spline (solid line) is fitted to the IR optical-depth values (diamonds). Vertical bars indicate the standard deviation.

Between 1315 and 1600 UTC a large section in the middle and lower parts of the cloud layer was observed where low depolarization ($\Delta < 0.2$) and strong backscattering coincided (cf. Fig. 4). Above that layer the depolarization ratio assumed typical values of greater than 0.2 most of the time. The depolarization measurements are consistent with the following explanation. In the upper part of the fully developed cloud, ice crystals were generated. They were too small to attain a horizontal alignment. Random orientation also dominates during falling if the maximum dimension of the crystals is less than 100 μm (Sassen 1980). Particles grew as they fell through the cloud. Due to their larger size, particles were predominantly horizontally aligned during falling in the middle and lower parts of the cloud deck. A circumzenithal arc observed with a fish-eye camera at Heligoland around 1400 UTC suggests that the scattering crystals were mainly plates. Below about the 9.5-km height, evaporation of ice-crystal trails took place. Particles got small again. Decreasing size and sedimentation velocity as well as turbulence effects, possibly present at cloud base, prevented an alignment of the particles.

Again during the dissolution process, starting at about 1515 UTC, descending layers were identified by small depolarization ratios just below the upper cloud rim (cf. Fig. 6 between 1515 and 1700 UTC); Δ partly remained greater than 0.2 in the lower part of the cirrus, but cloud segments with $\Delta < 0.1$ were now also present.

The absence of strong winds and turbulence has presumably favored the quiescent evolution of the cloud deck as suggested by the depolarization measurement.

c. *Cirrus geometrical and optical properties*

Before the discussion of geometrical and transmission properties, a two-wavelength measurement is presented in Fig. 7. The experiment was made at Sylt to check the wavelength dependence of cirrus particle scattering. Because no absolute calibration of the signals at the two wavelengths was carried out, only changes of the ratio $P(z, 550\text{ nm})/P(z, 728\text{ nm})$ with height, as given in Fig. 7, can be interpreted. The optical depth of the 4-km deep cirrus was 0.1 so that the signal ratio only depends on the backscatter coefficient ratio according to the discussion in section 4d. A range-independent signal ratio inside the two cirrus layers implies a constant wavelength behavior of ice-crystal scattering with height. A λ^0 dependence of cirrus scattering is indicated by the increase of the signal ratio from 1 at cloud base to 2.85 at 5.7 km, where the signal ratio attains its maximum. The increase by 1.85 results in the reasonable value of 0.05 for the particle-to-molecular backscatter ratio in the upper troposphere (Russel et al. 1979) below a cirrus cover at a wavelength of 725 nm if particle backscattering inside and below the cloud is proportional to λ^0 and λ^{-1}, respectively. The measured difference of 1.85 is less consistent with a λ^{-1} or $\lambda^{-0.5}$ dependence of cirrus scattering, because

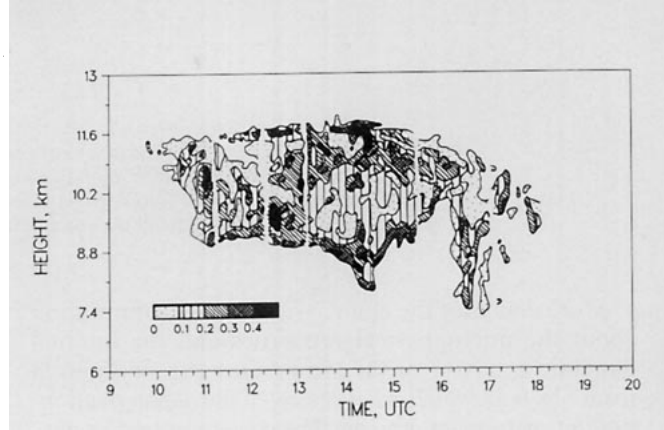

FIG. 6. Height–time display of the depolarization ratio observed at Heligoland on 18 October 1989. The corresponding range-corrected backscatter signal is shown in Fig. 4. Range and time resolution are 15 m and 2 min.

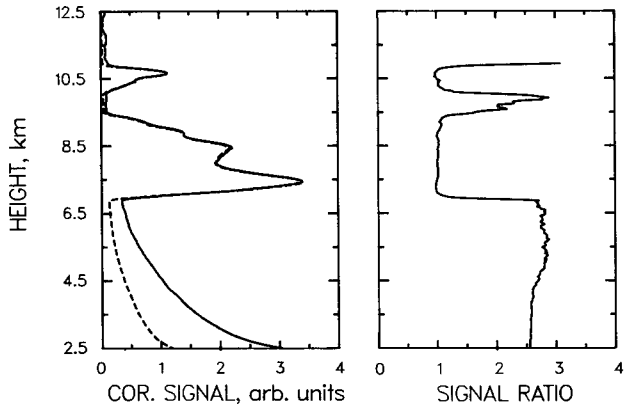

FIG. 7. Two-wavelength measurement of cirrus particle backscattering performed with the DIAL at Sylt 1842 UTC 18 October 1989. Sampling time is 10 min. The simultaneously measured and range-corrected signals for the wavelengths of 550 nm (solid line) and 728 nm (dashed line) are smoothed with a sliding average window length of 240 m. The 550-nm backscatter signal is fitted such that the signal ratio $P(z, 550\text{ nm})/P(z, 728\text{ nm}) = 1$ at cirrus cloud base.

then a particle-to-Rayleigh backscatter ratio of 0 or 0.01 results for the height of 5.7 km, which appears to be unrealistically small. A signal ratio of about 2.5 observed between 2.5 and 4.5 km corresponds to a particle-to-molecular backscatter ratio of 0.2 for the assumptions made above; $\beta_{aer}/\beta_{mol} = 0.2$ is typical for the lower troposphere above the boundary layer.

All these facts indicate λ^0 behavior of cirrus scattering. Thus, no wavelength corrections have been made to the results presented in Fig. 8, in which time series of cloud depth, optical thickness, and of mean cloud extinction-to-backscatter ratio are shown. The calculated cloud depth is obtained by taking the difference of cloud-top and cloud-base heights and subtracting layers inside the cloud for which condition (2) is not fulfilled. Forward and backward integration is applied in the evaluation of lidar data collected at Norderney. Because sufficiently accurate lidar signals from above the tropopause could not be measured at Heligoland and Sylt, forward integration alone had to be carried out. The technique suggested by Platt (1979) (cf. section 4b) could be used in the determination of the cirrus optical properties over Heligoland in most cases. Only at the beginning and at the end of the observation period was forward integration stable for any lidar ratio, at least below 100 sr. Here a fixed but reasonable lidar ratio of 15 sr was chosen in the calculations. A time-invariant lidar ratio of 15 sr was also used in the evaluation of the entire lidar dataset sampled at Sylt because cirrus optical depth was 0.1 or less most of the time. Platt's method could not be applied here.

Figure 7 shows that, for Sylt, particle backscatter was very weak just below the cirrus and also negligible above the cloud. This observation holds for the other lidar sites as well, including Norderney, so that the use of a boundary value $\beta_{aer}(z_0) = 0$ is justified.

The relative error of the cirrus optical depth in Fig. 8 is roughly equal to the relative error of the S_{aer} estimate. The uncertainty is small in cases where the cirrus lidar ratio could be determined from measurements, but of the order of 50%–100% if the lidar ratio had to be guessed.

A small underestimation of the cirrus optical depth of up to 10% for RFOVs of 0.5 mrad or less (Sylt, Norderney) and of 20% for a RFOV around 2 mrad (Heligoland) must be considered in Fig. 8 due to multiple scattering. The effect is estimated by using an algorithm developed by Eloranta and Shipley (1982), a phase function for ice-crystal scattering given by Takano and Liou (1989) for cirrostratus, and the cirrus characteristics as shown in Figs. 4 and 8.

Figure 8 illustrates the development of the cloud system in terms of the optical and geometrical depths. The evolution was similar at Heligoland and Norder-

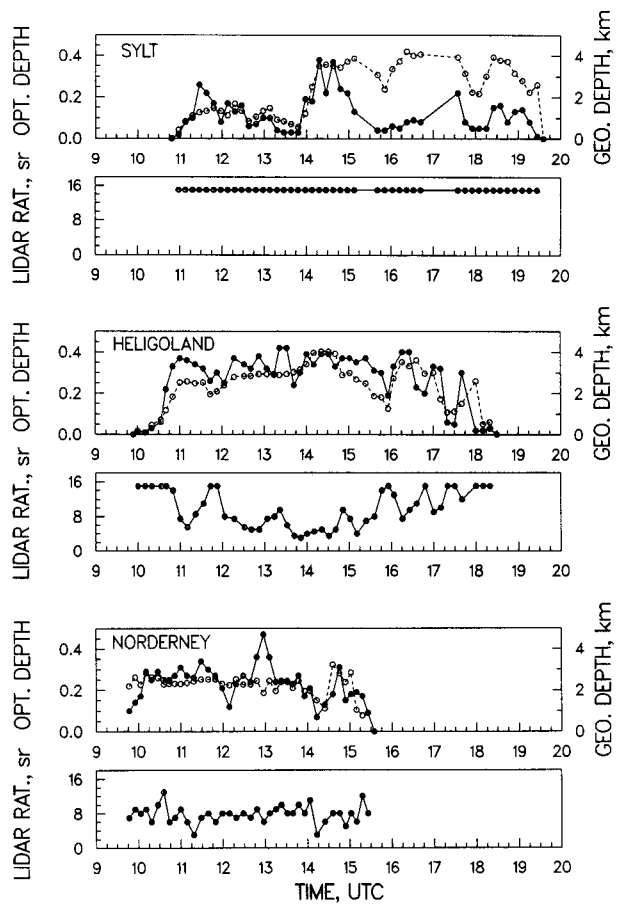

FIG. 8. Time series of cloud optical (closed circles) and geometrical depth (open circles) and of the cloud lidar ratio (Heligoland and Norderney) for the cirrus cloud deck observed on 18 October 1989. Ten-minute average values are calculated.

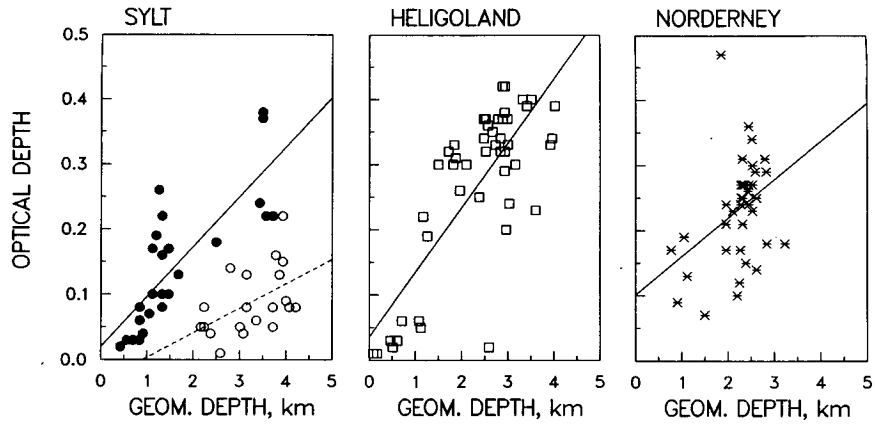

FIG. 9. Geometrical versus optical depth. Least-squares regression lines are fitted to the data shown as time series in Fig. 8. The time series observed at Sylt is split into intervals from 1045 to 1500 UTC (closed circles, solid line) and from 1500 to 1930 UTC (open circles, dashed line). Correlation coefficients are 0.80 (Sylt, solid line), 0.50 (Sylt, dashed line), 0.79 (Heligoland), and 0.38 (Norderney).

ney. About one hour after the occurrence of first cirrus a completely developed cloud deck was observed. Then the vertical extension varied smoothly (Norderney) or increased slightly with time (Heligoland) before dissolution began at about 1400 and 1500 UTC, respectively.

The good correlation between cloud depth and optical depth is obvious from Fig. 9. Nearly the same mean cloud extinction coefficient, that is, ratio of cloud optical-to-geometrical depth, was observed at Heligoland and Norderney, and also at the Sylt site until 1500 UTC (cf. Figs. 8 and 9). Its value was roughly 0.1 km^{-1}. In other respects, cloud behavior over Sylt differed considerably from findings at the other lidar stations. After a rapid increase of both the geometrical and optical depths between 1345 and 1430 UTC, the optical thickness decreased again back to low values around 0.1 as had been observed before 1345 UTC, while cloud vertical extension remained large. Drier air masses may then have reached the site, causing the dissolution of the cirrus and leading to the rapid decrease of particle size and optical depth.

The time series of the extinction-to-backscatter ratio in Fig. 8 calculated from the Heligoland lidar data confirms the interpretation of the depolarization measurements. The lidar ratio was small in the middle of the observation period, especially between 1330 and 1445 UTC, when also low depolarization ratios and strong backscatter signals were measured (cf. Figs. 4 and 6); $S_{aer} < 5$ sr is best explained by specular reflection from falling particles causing a very large backscatter coefficient. The low depolarization and very low lidar ratios observed at Heligoland over large time sections suggest that a considerable amount of large particles was present in the cirrus here. As was already mentioned, ice plates with maximum dimension of greater than 100 μm possess the optimum size for a horizontal alignment. The absence of lidar ratios less than 5 sr most of the time over Norderney suggests that the particles were too small to assume a stable horizontal orientation while falling. Aircraft measurements performed over Norderney between 1300 and 1400 UTC indicated the presence of particles predominantly smaller than 50 μm. Random orientation of crystals was found to lead to lidar ratios between 5 and 20 sr (Ansmann et al. 1992b). Numerical calculations by Takano and Liou (1989) indicate values of around 10 sr in this case.

Figure 10 summarizes statistical results of the cirrus observations made on 18 October 1989. All data are calculated from 10-min lidar-signal averages. Because of the coincidence of cirrus top and tropopause heights, the average top height was roughly equal at all field

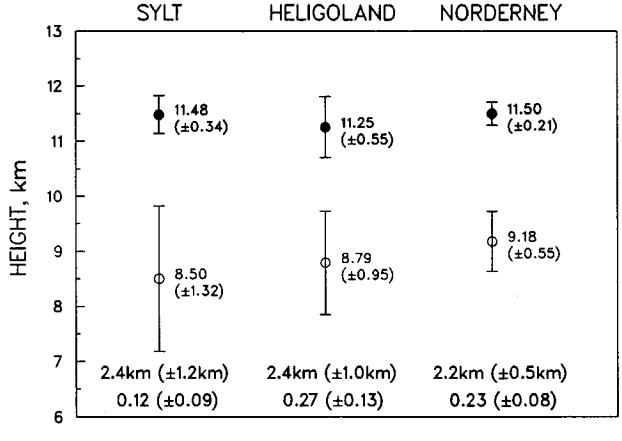

FIG. 10. Statistical analysis of cloud-top and cloud-base heights, 10-min signal averages. Vertical bars indicate standard deviations, also given as numbers in parentheses. The mean values and the standard deviations of the geometrical and optical depths calculated from the respective time series as given in Fig. 8 are shown at the bottom.

sites. As is typical for cirrus, cloud base varied strongly compared to the cloud top. Ice-crystal trails caused the difference in behavior. The base height lowered from Norderney over Heligoland to Sylt. While, on average, cloud depths were equal at the different field sites, cirrus optical depths measured at the neighboring islands of Heligoland and Sylt differed by a factor of 2.

The three-lidar observation nicely shows that cloud evolution was similar over the different observation sites during the passage of a band of moist air with a west-to-east extension of roughly 300–350 km, but also that the cloud structures and the scattering and microphysical properties can change rapidly in both time and space.

6. Statistical analysis

By the use of the lidar-radiosonde network a large number of quasi-simultaneous measurements of cloud-base and cloud-top heights, geometrical and optical depths, and temperature profiles in the cloud layer were sampled within a short time period. Data on 38 different cirrus systems could be collected between 5 September and 27 October 1989. The essential results of the statistical analysis are presented in this section. Lidar and radiosonde measurements made before and after ICE in northern Germany indicate that the findings are roughly representative for all seasons of the year, not only for the fall season.

Eighty percent of the ice clouds were advected from the west, that is, from the North Sea or the Atlantic, so the results may give a view inside the behavior of marine ice clouds at latitudes between 50° and 60°N. In 45% of the cases cirrus occurred only for a short time period, between 10 and 60 min. Cirrus fields present for more than 3 h and up to 12 h were observed in 9 of the 38 cases.

Figure 11 shows the frequency of occurrence of mean cloud-top heights, of cirrus-top temperatures, and of mean temperature gradients between cloud base and top. As cirrus begins to form at the top of a humid layer, the figure indicates at which heights and temperatures cirrus formation preferably starts. Mean cloud-top heights were typically above 10 km and coincided in 40% of the observations with the tropopause height. One can conclude that, in most cases, first cirrus generation cells occurred just below the tropopause, at temperatures below −50°C.

Compared to the top height, the base height was found to be rather evenly distributed between 7 and 10 km, since especially the cloud base lowers with time due to descending ice-crystal layers, as was illustrated in Fig. 10. Mean cloud temperatures, defined as the average of mean cloud-base and mean cloud-top temperatures, were mainly between −40° and −55°C.

The analysis of cloud temperature gradients indicates that, on average, statically stable conditions prevailed in cirrus clouds. In about 75% of the cases, gradients between 7° and 9°C km^{-1} were observed.

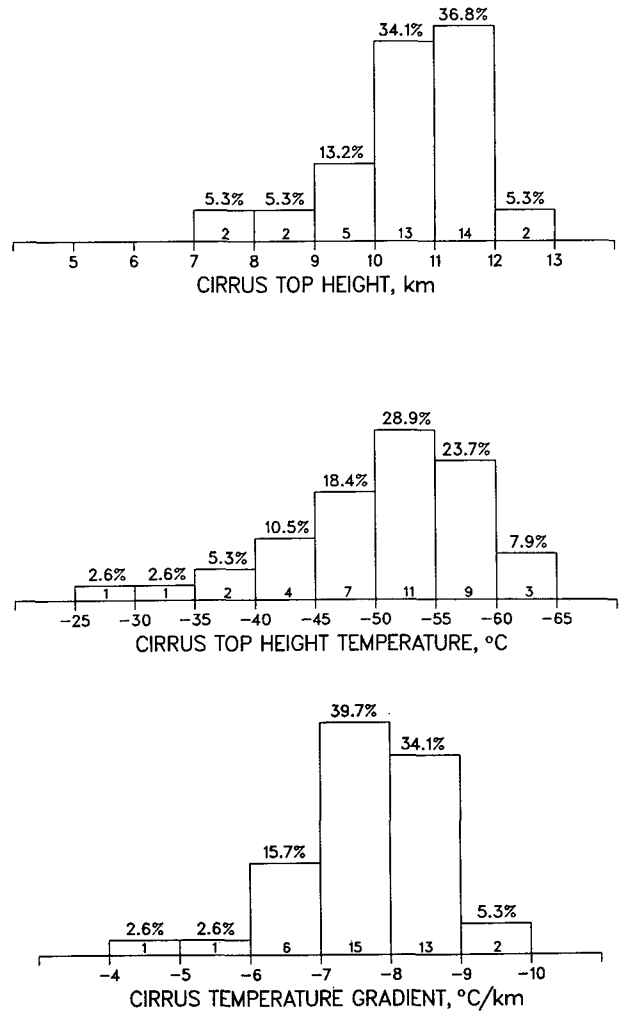

FIG. 11. Distribution of mean top heights, top-height temperatures, and mean cloud temperature gradients of 38 cirrus clouds observed with the ICE lidar network. The number of observations for a range, temperature, or temperature gradient interval is given at the bottom of the corresponding column.

Frequency distributions of cloud optical and geometrical depths and the relation between mean cloud optical and geometrical depth are given in Fig. 12. In 28 of the 38 cases the mean vertical extension was between 0.5 and 1.8 km, and the optical depth varied between 0.05 and 0.35. Small cloud depths of less than 1.0 km were typically observed in cases where cirrus appeared for less than one hour. Only when cloud evolution lasted longer than about 1.5 h, significant cloud-base lowering initiated by ice-crystal fallstreaks was found to take place. The largest mean cloud depths occurred in cirrus decks lasting longer than several hours. In six of a total of seven observations with mean cloud depth larger than 2.5 km, cirrus began to form at heights above 11.5 km and persisted for more than four hours.

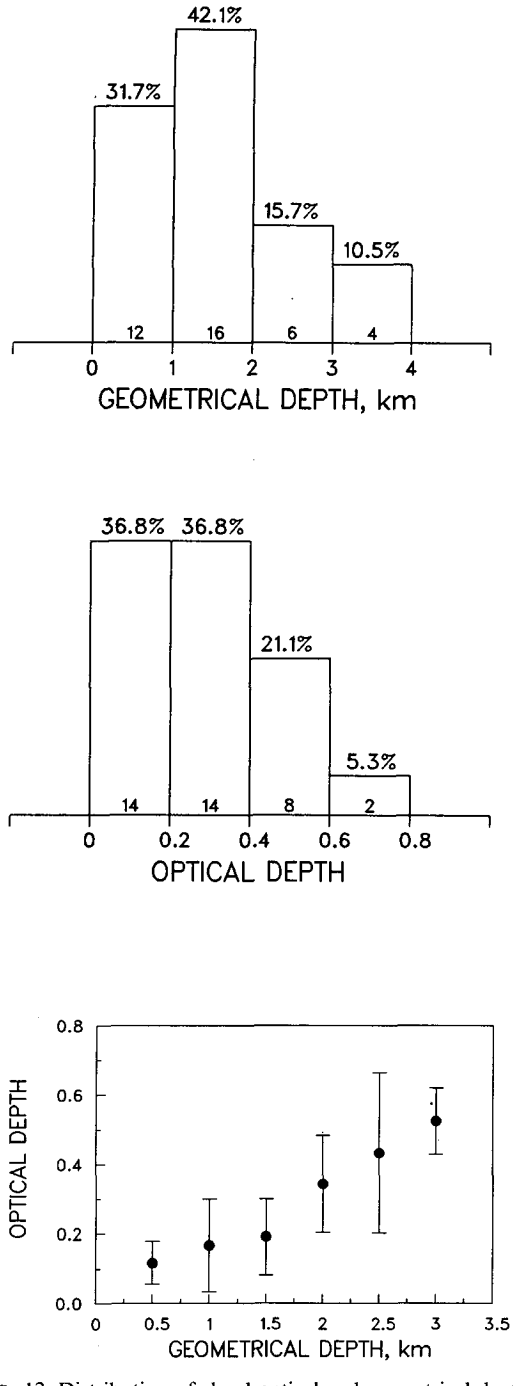

FIG. 12. Distribution of cloud optical and geometrical depths of 38 cirrus systems, and the relation between both quantities. The number of observations for a cloud-depth or an optical-depth interval is given at the bottom of the corresponding column. Values are grouped in 0.5-km intervals in the correlation plot. Standard deviations are indicated by vertical bars.

The good correlation between cloud depth and optical depth probably results from the fact that the measured cloud extinction coefficients are small, on the order of 0.15 km^{-1} (cf. Fig. 13). As a consequence, ice water content and microphysical properties cannot vary strongly with time, which is certainly favorable for a good correlation.

The dependence of cloud optical and geometrical depths and of the mean cloud extinction coefficient on midcloud temperature is illustrated in Fig. 13. No significant relationship between geometric cloud depth and temperature is found, presumably due to the fact that mean cloud depths were, in general, small. Such thin clouds can occur at all heights in the upper troposphere.

Although the variations are large (cf. Fig. 13, vertical bars), a dependence of the mean cloud optical thickness on temperature can be noticed. Ice water content and, thus, extinction by ice crystals increases with increasing

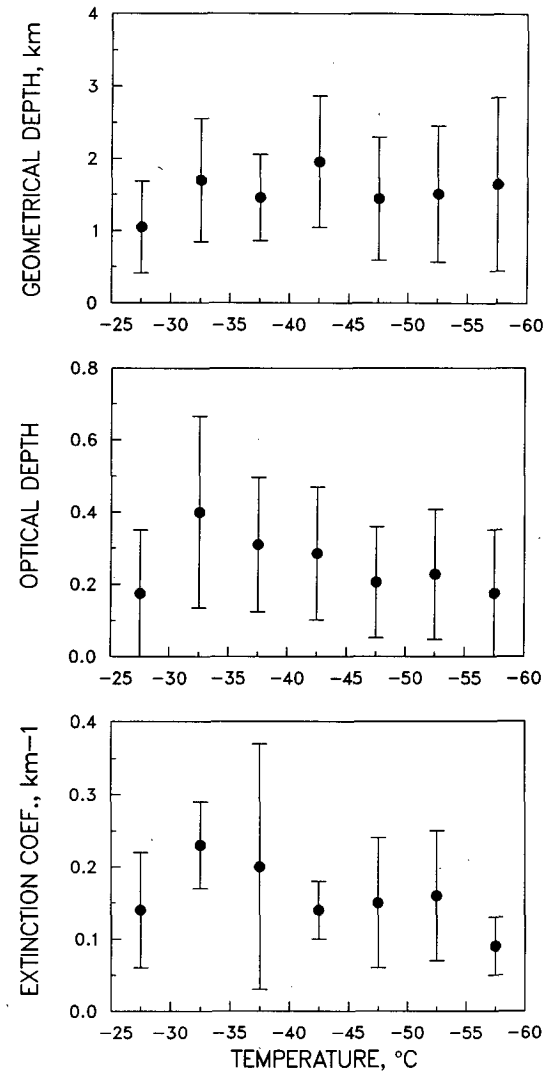

FIG. 13. Mean values (closed circles) of cloud depth, cloud optical depth, and cloud extinction coefficient (optical depth/geometrical depth) versus midcloud temperature. Standard deviations are indicated by vertical bars. Values are grouped in intervals of 5°C.

temperature and water vapor pressure. The lower boundary of the height range where cirrus can occur is also determined by temperature. Cirrus with mid-cloud temperatures greater than −30°C and corresponding cloud center around 7 km must be at least geometrically thin, and were usually also found to be optically thin (cf. Fig. 13).

The distribution of mean cloud extinction coefficients underlines the essential findings discussed above. For the typical cirrus temperature range between −40° and −55°C, the average cirrus extinction coefficient is about 0.15 km^{-1}.

7. Summary

A mesoscale lidar network has been used to measure cirrus cloud properties over the North Sea in September and October 1989. The instruments employed had not been specially designed for this experiment and were in fact quite different. Laser wavelengths ranged between 308 and 1064 nm. On the other hand, the different types of lidars allowed several special measurements. A two-wavelength measurement of cirrus particle backscattering confirmed the wavelength independence of ice-crystal scattering so that optical properties measured with the lidar net could be compared without any assumptions about the wavelength behavior of cirrus scattering.

Results of a case study are presented. A complete life cycle of a cirrus system was monitored with lidars and radiosondes on one of the ICE '89 key days. Height–time displays of particle backscatter show that the cloud cover was fully developed within less than 1 h. The dissipation began about 3 h before the last cloud segments dissolved. It was often observed during ICE '89 that the cloud top stayed approximately constant, while the cloud base lowered with time due to ice-crystal trails. Although a similar cloud evolution behavior was found at the different lidar stations, cloud structures and scattering properties differed between sites.

Probably due to the absence of strong winds and turbulence, low depolarization ratios were measured over long time periods in the center part of the cloud deck, indicating layers with falling crystals. The quiescent cloud evolution is believed to be the reason for the observed good correlation between cloud optical and geometrical depth. Cloud extension and optical thickness varied smoothly most of the time.

The essential results of a statistical analysis based on 38 different cirrus cases collected during ICE '89 are presented. The results show that 80% of the ice clouds were advected from the west and associated with warm-front passages.

Cirrus typically began to form between 10 and 12.5 km at temperatures between −50° and −65°C. Statically stable conditions prevailed in cirrus. Mean cloud temperature gradients between 6° and 9°C km^{-1} were found in 90% of all cases.

Most of the observed cloud systems were thin with mean optical depths less than 0.4, geometrical depths less than 2 km, and a mean cloud extinction coefficient between 0.1 and 0.2 km^{-1}. A good correlation between mean cloud optical and geometrical depth is found.

A weak dependence of the mean cloud optical depth and the mean cloud extinction coefficient on temperature and, thus, on water vapor pressure was observed.

The lidar network used in the ICE '89 cooperation thus provided a large body of data about geometric and radiometric properties of cirrus clouds. The simultaneous observation of the same cloud deck with three lidars yielded valuable information on the temporal, vertical, and horizontal behavior of cirrus in mesoscale dimensions.

Acknowledgments. The successful operation of several complex instruments in the frame of a large field experiment depended on the help and cooperation of many people and organizations. Only some of them can be named explicitly, but we are particularly grateful to all the others as well.

From the MPI group many thanks are due to the Standortverwaltung Westerland and the commander and staff of the Pidder-Lüng-Kaserne in Hörnum, who provided an excellent platform and support for our experiment. The group also would like to thank F. Jonas, R. Kapp, M. Pfeiffer, and V. Rohde for their aid in setting up the system. The work was supported by the Bundesminister für Forschung und Technologie under Grant KF 10110.

The DWD group acknowledges the cooperation and support of the Biologische Anstalt Helgoland and the Institut für Meereskunde (IfM), Kiel. Radiosonde measurements were performed by IfM. The participation of these groups was partially funded by the Institut für Geophysik und Meteorologie, Cologne.

The LMD group is grateful to C. Loth and J. Pelon for their contributions to the field experiment phase and discussions during the data analysis process.

The GKSS group gratefully acknowledges help by the Wasserwerke Norderney during the planning and measurement phase of the experiment. They also wish to thank H. O. Boie and collaborators for the design and construction of the mechanical and electrical installation, as well as H. Westermann and T. Weitkamp for their support during the intensive field phase.

The assistance of H. Luthardt of Deutsches Klimarechenzentrum Hamburg in preparing the height–time displays of the backscatter coefficient is appreciated.

REFERENCES

Ansmann, A., M. Riebesell, U. Wandinger, C. Weitkamp, E. Voss, W. Lahmann, and W. Michaelis, 1992a: Combined Raman elastic-backscatter lidar for vertical profiling of moisture, aerosol extinction, backscatter, and lidar ratio. *Appl. Phys. B*, **55**, 18–28.

——, U. Wandinger, M. Riebesell, C. Weitkamp, and W. Michaelis, 1992b: Independent measurement of extinction and backscatter profiles in cirrus clouds by using a combined Raman elastic-backscatter lidar. *Appl. Opt.*, **31,** 7113–7131.

Bösenberg, J., A. Ansmann, S. Elouragini, P. H. Flamant, K. Klapheck, H. Linné, C. Loth, L. Menenger, W. Michaelis, P. Moerl, J. Pelon, W. Renger, M. Riebesell, C. Senff, P.-Y. Thro, U. Wandinger, and C. Weitkamp, 1990: Measurements with lidar systems during the International Cirrus Experiment 1989. MPI report no. 60, Max-Planck-Institut für Meteorologie, Bundesstrasse 55, 20146 Hamburg, Germany, 152 pp.

——, 1991: A differential absorption lidar system for high resolution water vapor measurements in the troposphere. MPI report no. 71, Max-Planck-Institut für Meteorologie, Bundesstrasse 55, 20146 Hamburg, Germany, 38 pp.

Eloranta, E. W., and S. T. Shipley, 1982: A solution for multiple scattering. *Atmospheric Aerosols—Their Formation, Optical Properties, and Effects,* A. Deepak, Ed. Spectrum Press, 227–239.

Fernald, F. G., 1984: Analysis of atmospheric lidar observations: Some comments. *Appl. Opt.*, **23,** 652–653.

van de Hulst, H. C., 1981: *Light Scattering by Small Particles.* Dover Publications, Inc., 470 pp.

Klett, J. D., 1981: Stable analytic inversion solution for processing lidar returns. *Appl. Opt.*, **20,** 211–220.

Liou, K. N., 1986: Influence of cirrus clouds on weather and climate processes: A global perspective. *Mon. Wea. Rev.*, **114,** 1167–1199.

——, and H. Lahore, 1974: Laser sensing of cloud composition: A backscattered depolarization technique. *J. Appl. Meteor.*, **13,** 257–263.

Platt, C. M. R., 1979: Remote sounding of high clouds: I. Calculation of visible and infrared optical properties from lidar and radiometer measurements. *J. Appl. Meteor.*, **18,** 1130–1143.

——, J. C. Scott, and A. C. Dilley, 1987: Remote sensing of high clouds. Part VI: Optical properties of midlatitude and tropical cirrus. *J. Atmos. Sci.*, **44,** 729–747.

——, J. D. Spinhirne, and W. D. Hart, 1989: Optical and microphysical properties of a cold cirrus cloud: Evidence for regions of small ice particles. *J. Geophys. Res.*, **94,** 11 151–11 164.

Raschke, E., D. Hennings, R. Sefzig, and M. Quante, 1990: International Cirrus Experiment: Field Phase Plan. *Institut für Geophysik und Meteorologie, Universität zu Köln,* 129 pp.

Russel, P. B., T. J. Swissler, and M. P. McCormick, 1979: Methodology for error analysis and simulation of lidar aerosol measurements. *Appl. Opt.*, **18,** 3783–3797.

Sassen, K., 1980: Remote sensing of planar ice crystals fall attitudes. *J. Meteor. Soc. Japan,* **58,** 422–429.

——, C. J. Grund, J. D. Spinhirne, M. M. Hardesty, and J. M. Alvarez, 1990: The 27–28 October 1986 FIRE IFO cirrus case study: A five lidar overview of cloud structure and evolution. *Mon. Wea. Rev.*, **118,** 2288–2311.

Schotland, R. M., K. Sassen, and R. Stone, 1971: Observations by lidar of linear depolarization ratios for hydrometeors. *J. Appl. Meteor.*, **10,** 1011–1017.

Takano, Y., and K. N. Liou, 1989: Solar radiative transfer in cirrus clouds. Part I: Single scattering and optical properties of hexagonal ice crystals. *J. Atmos. Sci.*, **46,** 3–19.

Theopold, F. A., and J. Bösenberg, 1993: Differential absorption lidar measurements of atmospheric temperature profiles: Theory and experiment. *J. Atmos. Oceanic Technol.*, **10,** 165–179.

Thomas, L., J. C. Cartwright, and D. P. Wareing, 1990: Lidar observations of the horizontal orientation of ice crystals in cirrus clouds. *Tellus,* **42b,** 211–216.